Timing Error Detector Design and Analysis for Quasi-Orthogonal Space-Time Block Coding

Pawel A. Dmochowski, Peter J. McLane
Department of Electrical and Computer Engineering
Queen's University, Kingston, ON, K7L 3N6, Canada
Email: pdmochowski@ieee.org, mclanep@post.queensu.ca

***Abstract*— Design and analysis of low complexity timing error detectors (TEDs) for quasi-orthogonal space-time block coding systems are presented. The detectors operate on data symbols and approximate decision variables, producing timing error measurement robust to channel fading. In addition to the estimator S-curve, we obtain the estimation error variance and TED SNR, with the analysis carried out under the assumptions of perfect data and channel knowledge at the receiver. Simulations are used to examine the effects of decision errors on the detector characteristics, and to evaluate the overall system performance, where the proposed TEDs are incorporated into the receiver timing loop. Receivers with perfect channel knowledge and pilot-based channel estimation are considered. Symbol error rate results show timing synchronization loss of less than 0.5 dB for a receiver with perfect channel information.**

I. Introduction

Timing acquisition in space-time coded modems was first addressed in [1], where the receiver obtained timing information by maximizing the oversampled log-likelihood function (LLF), derived from orthogonal training sequences. It has been shown [2], that the algorithm in [1] is highly sensitive to the oversampling ratio used. Modifications reducing the required oversampling have been presented in [2], [3].

In contrast to the work described above, which deals primarily with the problem of maximum-likelihood (ML)-based timing acquisition using a training preamble, we consider the problem of timing error detector (TED) design for low complexity timing error tracking. A TED for Alamouti orthogonal space-time block coding (OSTBC) was presented and analyzed in [4], [5], with the theory subsequently generalized to higher order OSTBC in [6]. In this sequel, we consider an extension of the TED design and analysis to quasi-OSTBC (QOSTBC). Analytical properties are derived assuming data and channel knowledge at the receiver, while the effects of erroneous data decisions and channel estimation errors are evaluated by means of simulations.

In what follows, the system overview is described in Section II, while Section III presents the theory of TED design and analysis for QOSTBC. System simulations evaluating the performance of QOSTBC receivers incorporating the designed TED are presented in Section IV. We conclude with a summary in Section V.

II. System Overview

Consider an OSTBC system with N_t transmit and N_r receive antennas, where the transmitter encodes N_s information symbols over N_t antennas in N_c time slots, resulting in a code rate of $R = N_s/N_c$. Using boldface notation for matrices, we denote the lth $N_t \times N_c$ code block by $\mathbf{X}_l$, and its (i,k)th entry by $x_i(lN_c + k)$. Note that l is the block index, $k = 0, \ldots, N_c - 1$ is the time slot within the block and $i = 1, \ldots, N_t$ is the transmit antenna index. One of the advantages of OSTBC systems lies in the fact that if the columns of $\mathbf{X}_l$ are orthogonal, the receiver complexity can be greatly reduced by decoupling the decoding process into N_s independent operations [7]. It has been shown, however, that the maximum rate for $N_t > 2$ is $R = 3/4$ [7]. In order to achieve rate one codes for $N_t > 2$, the property of full code orthogonality must be relaxed, resulting in *quasi*-OSTBC. QOSTBCs have been been shown [8] to provide only half of the maximum diversity order, and to address this shortcoming a subset of the data symbols is drawn from a constellation rotated by an angle ϕ, resulting in a ϕ-QOSTBC system [8]. Denoting the mth information symbol encoding block $\mathbf{X}_l$ by a_m^l, where $m = 0, \ldots, N_s - 1$, and considering a $N_s = 4$ without loss of generality, we have

$$\tilde{a}_m^l = \begin{cases} a_m^l & m = 1, 2 \\ a_m^l e^{j\phi} & m = 3, 4. \end{cases}$$

The encoding process for $\mathbf{X}_l$ can be expressed by [9],

$$\mathbf{X}_l = \sum_{m=0}^{N_s-1} \Re\{a_m^l\}\mathbf{A}_m + i\Im\{a_m^l\}\mathbf{B}_m, \tag{1}$$

where the operators $\Re\{\cdot\}$ and $\Im\{\cdot\}$ return the real and imaginary parts of their arguments, respectively, and $\mathbf{A}_m$ and $\mathbf{B}_m$ are integer code matrices of dimension $N_t \times N_c$. An example of a $N_t = 4$ antenna QOSTBC is given by [8]

$$\mathbf{X}_{(q4)} = \begin{bmatrix} a_1 & -a_2^* & -a_3^* & a_4 \\ a_2 & a_1^* & -a_4^* & -a_3 \\ a_3 & -a_4^* & a_1^* & -a_2 \\ a_4 & a_3^* & a_2^* & a_1 \end{bmatrix}. \tag{2}$$

Following data encoding, the pulse shaping is split between the transmitter and the receiver, each employing a root raised cosine (RRC) filter. The combined Nyquist raised cosine pulse is represented by $g(t)$. We assume a frequency-flat Rayleigh fading channel modeled by a $N_r \times N_t$ matrix $\mathbf{H}$. It's components, denoted by h_{ji}, correspond to the state of the channel from ith transmit to jth receive antenna and are assumed to be

independent and identically distributed (iid) with a U-shaped power spectrum and maximum symbol-normalized Doppler frequency of $f_D T$, assumed to be known.

The receiver diagram is given in Figure 1. We assume that

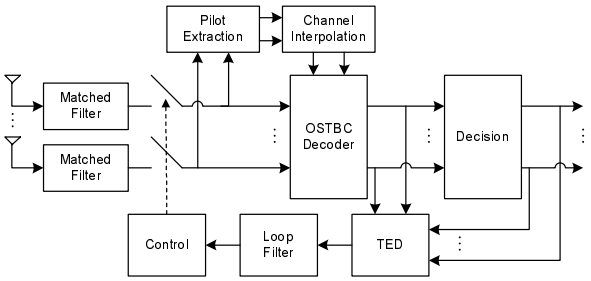

Fig. 1. Receiver Diagram.

the received signal is sampled with a timing error ϵ equal on all branches and constant for the duration of $\mathbf{X}_l$. We model ϵ by $\epsilon = \tau - \hat{\tau}$ where τ is the timing offset at the receiver and $\hat{\tau}$ is the timing correction applied by the timing synchronization algorithm. It was shown in [6] that the lth $N_r \times N_c$ received matrix $\mathbf{Y}_l$ is given by

$$\mathbf{Y}_l = \mathbf{H}_l \sum_n \mathbf{X}_{l+n} \mathbf{G}_{\epsilon,n} + \mathbf{N}_l, \tag{3}$$

where $\mathbf{H}_l$ and $\mathbf{N}_l$ denote the channel state and noise matrices, respectively, and $\mathbf{G}_{\epsilon,n}$ is a $N_c \times N_c$ Toeplitz matrix given by

$$\mathbf{G}_{\epsilon,n} = \begin{bmatrix} g^{\epsilon}_{-nN_c} & g^{\epsilon}_{-nN_c+1} & g^{\epsilon}_{-nN_c+2} & \cdots \\ g^{\epsilon}_{-nN_c-1} & g^{\epsilon}_{-nN_c} & g^{\epsilon}_{-nN_c+1} & \ddots \\ g^{\epsilon}_{-nN_c-2} & g^{\epsilon}_{-nN_c-1} & g^{\epsilon}_{-nN_c} & \ddots \\ \vdots & \ddots & \ddots & \ddots \end{bmatrix},$$

where $g^{\epsilon}_n \triangleq g(nT+\epsilon)$. The summation in (3), marks the effects of intersymbol interference (ISI) due to ϵ, where $\mathbf{G}_{\epsilon,n} \to \mathbf{0}$ for large $|n|$.

The decoding is accomplished by means of optimization of the ML metric. Due to the partial orthogonality properties of the QOSTBC codes, the ML metric can be decomposed into a sum of independent terms. For the code given in (2), the metric is given by [8]

$$\mathcal{M} = f_{14}(s_1, s_4) + f_{23}(s_2, s_3), \tag{4}$$

where $f_{14}(s_1, s_4)$ and $f_{23}(s_2, s_3)$ are derived in [8].

III. Timing Error Detector

A. Timing Error Detector Design

It was shown in [6], [10], that for an OSTBC system, a measurement of ϵ, can be obtained using data symbols (or decisions) and decision variables. The average of the TED output represents the timing error measurement (TEM), referred to as the S-curve. As described in [6], the TEM in the form of $\hat{\epsilon} = g^{\epsilon}_{-1} - g^{\epsilon}_{1}$ returns a linear measurement of ϵ, referred to as the *difference of threshold crossings*. We now show, that a similar method can be used to design TEDs for ϕ-QOSTBC, with the modification to QOSTBC obtained by setting $\phi = 0$.

We note that an OSTBC receiver utilizes explicit expressions for the decision variables, which were subsequently used for TEM estimation in [6]. Due to the fact that the QOSTBC ML decoding in (4) cannot be fully decoupled, no explicit decision variables are available for TED design. Thus, in what follows, we use approximate decision variables, analogous to the OSTBC expressions, that is

$$\tilde{\zeta}_m = \|\mathbf{H}\|^{-2} \big[\Re\{\mathrm{tr}(\mathbf{Y}^H \mathbf{H} \mathbf{A}_m)\} - j\Im\{\mathrm{tr}(\mathbf{Y}^H \mathbf{H} \mathbf{B}_m)\} \big]. \tag{5}$$

One can show that $\tilde{\zeta}_m$ can be expressed as the decision variable s_m with a perturbation δ_{ζ_m}, that is

$$\tilde{\zeta}_m = s_m + \delta_{\zeta_m}, \tag{6}$$

where, for the example code in (2), the perturbation terms δ_{ζ_m} are given by [10, Chapter 6]

$$\begin{aligned} \delta_{\zeta_1} &= 2\|\mathbf{H}_l\|^{-2} \sum\nolimits_{j=1}^{N_r} \Re(h_{j1} h^*_{j4} - h^*_{j2} h_{j3}) s_4 \\ \delta_{\zeta_2} &= -2\|\mathbf{H}_l\|^{-2} \sum\nolimits_{j=1}^{N_r} \Re(h_{j1} h^*_{j4} - h^*_{j2} h_{j3}) s_3 \\ \delta_{\zeta_3} &= -2\|\mathbf{H}_l\|^{-2} \sum\nolimits_{j=1}^{N_r} \Re(h_{j1} h^*_{j4} - h^*_{j2} h_{j3}) s_2 \\ \delta_{\zeta_4} &= 2\|\mathbf{H}_l\|^{-2} \sum\nolimits_{j=1}^{N_r} \Re(h_{j1} h^*_{j4} - h^*_{j2} h_{j3}) s_1. \end{aligned}$$

We note that the numerator of δ_{ζ_m} contains only cross product terms in h_{ji}, while the denominator contains magnitude terms. It will be shown that by virtue of the iterative operation of the receiver timing loop, the effect of δ_{ζ_m} will be small, allowing for a valid timing error measurement. We stress, that the variables $\tilde{\zeta}_m$ are used strictly for the purpose of TEM estimation, while the data decisions s_m are obtained from (4). Finally, the use of (5) allows a semi-analytical derivation of the TED mean and estimation variance.

Similarly to the approach in [6], we consider a general expression for the TED output given by

$$\hat{\epsilon} = \Re\Big(\sum_k \alpha_k \tilde{a}_{n_{\alpha,k}} \tilde{\zeta}_{m_{\alpha,k}} + \beta_k \tilde{a}^*_{n_{\beta,k}} \tilde{\zeta}_{m_{\beta,k}} \Big), \tag{7}$$

with $\tilde{\zeta}_m$ given by (5). In the design process we aim to select the parameter set, that is,

$$\mathcal{S} = \{\alpha_k, \beta_k, m_{\alpha,k}, n_{\alpha,k}, m_{\beta,k}, n_{\beta,k}\}, \tag{8}$$

such that the S-curve, the average of the TED in (7), is in the form of a difference of threshold crossings TEM $g^{\epsilon}_{-1} - g^{\epsilon}_{1}$. The TED is the input to the timing loop which performs the required averaging.

We evaluate the expectation of (7), beginning with the expectation over data and the noise conditioned on the channel response, followed by the expectation over $\mathbf{H}$. In order to maintain compact notation, we denote the expectation conditioned on $\mathbf{H}$ by $E^{\mathbf{H}}\{\cdot\}$, while the expectation over $\mathbf{H}$ will be denoted by $E_{\mathbf{H}}\{\cdot\}$. Total expectation is thus given by

$E\{\cdot\} = E_{\mathbf{H}}\{E^{\mathbf{H}}\{\cdot\}\}$, where $E_{\mathbf{H}}\{\cdot\}$ is always computed by simulation as the argument is too complex for analysis.

Following an approach similar to that for OSTBC in [6], as shown in the Appendix, the expectation of the individual components in (7) is given by

$$\begin{aligned}\Re\{E^{\mathbf{H}}\{\tilde{a}_n\tilde{\zeta}_m\}\} &= \rho_2\|\mathbf{H}\|^{-2}\times \\ &\quad \mathrm{tr}\big\{(\mathbf{A}_m\mathbf{G}_\epsilon^H\mathbf{A}_n^H - \mathbf{B}_m\mathbf{G}_\epsilon^H\mathbf{B}_n^H)\Re(\mathbf{H}^H\mathbf{H})\big\}.\end{aligned} \tag{9}$$

Similarly, one can show that

$$\begin{aligned}\Re\{E^{\mathbf{H}}\{\tilde{a}_n^*\tilde{\zeta}_m\}\} &= \rho_2\|\mathbf{H}\|^{-2}\times \\ &\quad \mathrm{tr}\big\{(\mathbf{A}_m\mathbf{G}_\epsilon^H\mathbf{A}_n^H + \mathbf{B}_m\mathbf{G}_\epsilon^H\mathbf{B}_n^H)\Re(\mathbf{H}^H\mathbf{H})\big\}.\end{aligned} \tag{10}$$

Using (9) and (10), we have that the S-curve, conditioned on $\mathbf{H}$, for a ϕ-QOSTBC TED in (7), is given by an expression identical to that obtained for OSTBCs in [6], that is

$$E^{\mathbf{H}}\{\hat{\epsilon}\} = \rho_2\,\|\mathbf{H}\|^{-2}\,\mathrm{tr}\left\{\mathbf{\Gamma}\Re\left(\mathbf{H}^H\mathbf{H}\right)\right\}, \tag{11}$$

where ρ_2 is a constellation dependent constant, defined by

$$\rho_p \triangleq E\{(a_i^R)^p\} = E\{(a_i^I)^p\},$$

and the matrix $\mathbf{\Gamma}$, dependent on $\mathcal{S}$ in (8), is given by

$$\begin{aligned}\mathbf{\Gamma} = \sum\nolimits_k \big[&\alpha_k\big(\mathbf{A}_{m_{\alpha,k}}\mathbf{G}_\epsilon^H\mathbf{A}_{n_{\alpha,k}}^H - \mathbf{B}_{m_{\alpha,k}}\mathbf{G}_\epsilon^H\mathbf{B}_{n_{\alpha,k}}^H\big) \\ &+\beta_k\big(\mathbf{A}_{m_{\beta,k}}\mathbf{G}_\epsilon^H\mathbf{A}_{n_{\beta,k}}^H + \mathbf{B}_{m_{\beta,k}}\mathbf{G}_\epsilon^H\mathbf{B}_{n_{\beta,k}}^H\big)\big].\end{aligned} \tag{12}$$

Examining (11) and (12), one notes that the S-curve of a TED in (7) is independent of the rotation angle ϕ. Because of the equivalence of (11) and (12) to the expressions obtained for OSTBC in [6], we use the same design rules as those derived for OSTBC. We conclude that if $\mathbf{\Gamma}$ satisfies [6]

$$\mathbf{\Gamma} = f(\mathbf{G}_\epsilon)\mathbf{I} + \mathbf{D},$$

where

1) $f(\mathbf{G}_\epsilon)$ is a scalar function of $\mathbf{G}_\epsilon$ returning a difference of threshold crossings (TEM) approximating $g_{-1}^\epsilon - g_1^\epsilon$
2) $\mathbf{D}$ is an antisymmetric matrix,

then

$$E^{\mathbf{H}}\{\hat{\epsilon}\} = \rho_2 f(\mathbf{G}_\epsilon). \tag{13}$$

Since (13) is independent of $\mathbf{H}$, such a TED is referred to as *robust* [6]. If only condition 1) is satisfied, then [6]

$$E^{\mathbf{H}}\{\hat{\epsilon}\} = \rho_2 f(\mathbf{G}_\epsilon) + \delta_{\hat{\epsilon}}, \tag{14}$$

where $\delta_{\hat{\epsilon}}$, dependent on $\mathbf{H}$, is referred to as the TEM *bias*, given by

$$\delta_{\hat{\epsilon}} = \rho\,\|\mathbf{H}\|^{-2}\sum_{m=1}^{N_t}\sum_{\substack{i=1\\ i\neq m}}^{N_t}\sum_{j=1}^{N_r} d_{mi}\Re\left(h_{ji}^* h_{jm}\right), \tag{15}$$

where d_{mi} denotes the (m,i)th entry of $\mathbf{D}$. We note that the numerator of (15) contains only channel cross product terms, while the denominator contains magnitude terms by virtue of $\|\mathbf{H}\|^2$. Thus, due to the averaging operation of the timing loop, the effect of the bias term will be small, resulting in a *quasi-robust* TED. For a robust TED, (13) does not require averaging over the $\mathbf{H}$, and thus (13) represents the TED S-curve. For a quasi-robust TED, the S-curve is obtained by computing the expectation of the bias $\delta_{\hat{\epsilon}}$ in (14) over the channel fading matrix $\mathbf{H}$, that is

$$E\{\hat{\epsilon}\} = \rho_2 f(\mathbf{G}_\epsilon) + E_{\mathbf{H}}\{\delta_{\hat{\epsilon}}\}, \tag{16}$$

where the expectation $E_{\mathbf{H}}\{\delta_{\hat{\epsilon}}\}$ is evaluated by simulation.

B. Estimation Error Variance

We now examine the estimation error variance of the TED in (7), that is

$$\sigma_{\hat{\epsilon}}^2 = E\{\hat{\epsilon}^2\} - \left[E\{\hat{\epsilon}\}\right]^2. \tag{17}$$

Examining (7), one notes that the solution to $E\{\hat{\epsilon}^2\}$ can be obtained by considering the expectations $E^{\mathbf{H}}\{\tilde{a}_i^R\tilde{a}_j^R\tilde{\zeta}_m^R\tilde{\zeta}_n^R\}$, $E^{\mathbf{H}}\{\tilde{a}_i^I\tilde{a}_j^I\tilde{\zeta}_m^I\tilde{\zeta}_n^I\}$ and $E^{\mathbf{H}}\{\tilde{a}_i^R\tilde{a}_j^I\tilde{\zeta}_m^R\tilde{\zeta}_n^I\}$. Due to the complexity of the analysis, the reader is referred to [10, Appendix C] for details of the derivations.

As shown in [10, Appendix C], $E^{\mathbf{H}}\{\tilde{a}_i^R\tilde{a}_j^R\tilde{\zeta}_m^R\tilde{\zeta}_n^R\}$ is given by

$$E^{\mathbf{H}}\left\{\tilde{a}_i^R\tilde{a}_j^R\tilde{\zeta}_m^R\tilde{\zeta}_n^R\right\} = \|\mathbf{H}\|^{-4}\,\mathrm{tr}\big\{\rho_2^2\tilde{\mathbf{\Phi}}_{ijmn}^{RR} + \rho_2\frac{N_0}{2}\tilde{\mathbf{\Delta}}_{ijmn}^{RR}\big\}, \tag{18}$$

where $\tilde{\mathbf{\Phi}}_{ijmn}^{RR}$ is given by (19) and

$$\tilde{\mathbf{\Delta}}_{ijmn}^{RR} = \begin{cases}0 & i\neq j\\ (\mathbf{A}_m\otimes\mathbf{A}_n)\mathbf{\Lambda}_N(\mathbf{\Omega}'_{\text{RR}} + \mathbf{\Omega}'_{\text{II}}) & i=j,\end{cases} \tag{20}$$

where $\mathbf{\Omega}_{ij}$ and $\mathbf{\Omega}'_{ij}$ are defined by

$$\begin{aligned}\mathbf{\Omega}_{\text{RR}} &= \Re(\mathbf{H}^H\mathbf{H})\otimes\Re(\mathbf{H}^H\mathbf{H}) \quad \mathbf{\Omega}_{\text{II}} = \Im(\mathbf{H}^H\mathbf{H})\otimes\Im(\mathbf{H}^H\mathbf{H})\\ \mathbf{\Omega}_{\text{RI}} &= \Re(\mathbf{H}^H\mathbf{H})\otimes\Im(\mathbf{H}^H\mathbf{H}) \quad \mathbf{\Omega}_{\text{IR}} = \Im(\mathbf{H}^H\mathbf{H})\otimes\Re(\mathbf{H}^H\mathbf{H})\end{aligned}$$

and

$$\begin{aligned}\mathbf{\Omega}'_{\text{RR}} &= \Re(\mathbf{H})\otimes\Re(\mathbf{H}) \quad \mathbf{\Omega}'_{\text{II}} = \Im(\mathbf{H})\otimes\Im(\mathbf{H})\\ \mathbf{\Omega}'_{\text{RI}} &= \Re(\mathbf{H})\otimes\Im(\mathbf{H}) \quad \mathbf{\Omega}'_{\text{IR}} = \Im(\mathbf{H})\otimes\Re(\mathbf{H}).\end{aligned}$$

The $N_cN_c\times N_rN_r$ matrix $\mathbf{\Lambda}_N$ is given by

$$\mathbf{\Lambda}_N(i,j) = \begin{cases}1 & i = nN_r+n+1, j = mN_c+m+1\\ 0 & \text{elsewhere}\end{cases}$$

for $n=0,\ldots,N_r-1$ and $m=0,\ldots,N_c-1$. In (19), we have defined constellation dependent constants

$$\begin{aligned}\rho'_p &\triangleq E\{(a_i^R)^p(a_i^I)^p\} \quad \rho''_\phi \triangleq E\{(\tilde{a}_i^R)^3(\tilde{a}_i^I)\}\\ \rho'_{2\phi} &\triangleq E\{(\tilde{a}_i^R)^2(\tilde{a}_i^I)^2\} \quad \rho_{4\phi} \triangleq E\{(\tilde{a}_i^R)^4\},\end{aligned}$$

which are evaluated in [10, Appendix C].

Similarly, the solution to $E^{\mathbf{H}}\{\tilde{a}_i^I\tilde{a}_j^I\tilde{\zeta}_m^I\tilde{\zeta}_n^I\}$ is given by [10, Appendix C]

$$E^{\mathbf{H}}\left\{\tilde{a}_i^I\tilde{a}_j^I\tilde{\zeta}_m^I\tilde{\zeta}_n^I\right\} = \|\mathbf{H}\|^{-4}\,\mathrm{tr}\big\{\rho_2^2\tilde{\mathbf{\Phi}}_{ijmn}^{II} + \rho_2\frac{N_0}{2}\tilde{\mathbf{\Delta}}_{ijmn}^{II}\big\}, \tag{21}$$

with $\tilde{\mathbf{\Phi}}_{ijmn}^{II}$ is given by (22) and

$$\tilde{\mathbf{\Delta}}_{ijmn}^{II} = \begin{cases}0 & i\neq j\\ (\mathbf{B}_m\otimes\mathbf{B}_n)\mathbf{\Psi}_N(\mathbf{\Omega}'_{\text{RR}} + \mathbf{\Omega}'_{\text{II}}) & i=j.\end{cases} \tag{23}$$

$$\tilde{\mathbf{\Phi}}^{RR}_{ijmn} = \begin{cases} \big(\mathbf{A}_m\mathbf{G}^H_{\epsilon,0}\otimes\mathbf{A}_n\mathbf{G}^H_{\epsilon,0}\big)\big(\mathbf{A}^H_j\otimes\mathbf{A}^H_i+\mathbf{A}^H_i\otimes\mathbf{A}^H_j\big)\mathbf{\Omega}_{\text{RR}} & i\neq j \\ \big(\mathbf{A}_m\mathbf{G}^H_{\epsilon,0}\otimes\mathbf{A}_n\mathbf{G}^H_{\epsilon,0}\big)\Big[(\frac{\rho_{4\phi}}{\rho_2^2}-1)\big(\mathbf{A}^H_i\otimes\mathbf{A}^H_i\big)\mathbf{\Omega}_{\text{RR}}+(\frac{\rho'_{2\phi}}{\rho_2^2}-1)\big(\mathbf{B}^H_i\otimes\mathbf{B}^H_i\big)\mathbf{\Omega}_{\text{II}} \\ +\frac{\rho''_\phi}{\rho_2^2}\Big(\big(\mathbf{A}^H_i\otimes\mathbf{B}^H_i\big)\mathbf{\Omega}_{\text{RI}}+\big(\mathbf{B}^H_i\otimes\mathbf{A}^H_i\big)\mathbf{\Omega}_{\text{IR}}\Big)\Big] & \\ +\sum_l\sum_{k=0}^{N_s-1}\big(\mathbf{A}_m\mathbf{G}^H_{\epsilon,l}\otimes\mathbf{A}_n\mathbf{G}^H_{\epsilon,l}\big)\big[\big(\mathbf{A}^H_k\otimes\mathbf{A}^H_k\big)\mathbf{\Omega}_{\text{RR}}+\big(\mathbf{B}^H_k\otimes\mathbf{B}^H_k\big)\mathbf{\Omega}_{\text{II}}\big] & i=j \end{cases} \tag{19}$$

$$\tilde{\mathbf{\Phi}}^{II}_{ijmn} = \begin{cases} \big(\mathbf{B}_m\mathbf{G}^H_{\epsilon,0}\otimes\mathbf{B}_n\mathbf{G}^H_{\epsilon,0}\big)\big(\mathbf{B}^H_j\otimes\mathbf{B}^H_i+\mathbf{B}^H_i\otimes\mathbf{B}^H_j\big)\mathbf{\Omega}_{RR} & i\neq j \\ \big(\mathbf{B}_m\mathbf{G}^H_{\epsilon,0}\otimes\mathbf{B}_n\mathbf{G}^H_{\epsilon,0}\big)\Big[(\frac{\rho_{4\phi}}{\rho_2^2}-1)\big(\mathbf{B}^H_i\otimes\mathbf{B}^H_i\big)\mathbf{\Omega}_{RR}+(\frac{\rho'_{2\phi}}{\rho_2^2}-1)\big(\mathbf{A}^H_i\otimes\mathbf{A}^H_i\big)\mathbf{\Omega}_{\text{II}} \\ -\frac{\rho''_\phi}{\rho_2^2}\Big(\big(\mathbf{A}^H_i\otimes\mathbf{B}^H_i\big)\mathbf{\Omega}_{\text{IR}}+\big(\mathbf{B}^H_i\otimes\mathbf{A}^H_i\big)\mathbf{\Omega}_{\text{RI}}\Big)\Big] & \\ +\sum_l\sum_{k=0}^{N_s-1}\big(\mathbf{B}_m\mathbf{G}^H_{\epsilon,l}\otimes\mathbf{B}_n\mathbf{G}^H_{\epsilon,l}\big)\big[\big(\mathbf{B}^H_k\otimes\mathbf{B}^H_k\big)\mathbf{\Omega}_{RR}+\big(\mathbf{A}^H_k\otimes\mathbf{A}^H_k\big)\mathbf{\Omega}_{\text{II}}\big] & i=j \end{cases} \tag{22}$$

Finally, the expectation $E^{\mathbf{H}}\{\tilde{a}^R_i\tilde{a}^I_j\tilde{\zeta}^R_m\tilde{\zeta}^I_n\}$, is given by

$$E^{\mathbf{H}}\Big\{\tilde{a}^R_i\tilde{a}^I_j\tilde{\zeta}^R_m\tilde{\zeta}^I_n\Big\} = \|\mathbf{H}\|^{-4}\,\text{tr}\big\{\mu_\phi\tilde{\mathbf{\Phi}}^{RI}_{ijmn}\big\}, \tag{24}$$

where

$$\begin{aligned}\tilde{\mathbf{\Phi}}^{RI}_{ijmn} =&\big(\mathbf{A}_m\mathbf{G}^H_{\epsilon,0}\otimes\mathbf{B}_n\mathbf{G}^H_{\epsilon,0}\big)\times \\ &\big(\big(\mathbf{A}^H_i\otimes\mathbf{B}^H_j\big)\mathbf{\Omega}_{\text{RR}}-\big(\mathbf{B}^H_j\otimes\mathbf{A}^H_i\big)\mathbf{\Omega}_{\text{II}}\big)\end{aligned} \tag{25}$$

and μ_ϕ is defined as

$$\mu_\phi = \begin{cases}\rho_2^2 & i\neq j \\ \rho'_{2\phi} & i=j.\end{cases}$$

Using the general results given by (18), (21) and (24), the estimation variance for a particular TED is obtained using (17) with $E\{\hat{\epsilon}\}$ computed via (11) and (12), where

$$E\{\hat{\epsilon}^2\} = E_{\mathbf{H}}\Big\{\|\mathbf{H}\|^{-4}\,\text{tr}\Big\{\rho_2^2\mathbf{\Sigma}_{\tilde{\mathbf{\Phi}}}+\rho_2\frac{N_0}{2}\mathbf{\Sigma}_{\tilde{\mathbf{\Delta}}}\Big\}\Big\}. \tag{26}$$

The expectation $E_{\mathbf{H}}\{\cdot\}$ must be carried out by simulation, as will be done in Section III-C. The quantities $\mathbf{\Sigma}_{\tilde{\mathbf{\Phi}}}$ and $\mathbf{\Sigma}_{\tilde{\mathbf{\Delta}}}$ correspond to the linear combinations of $\tilde{\mathbf{\Phi}}^{RR}_{ijmn}$, $\tilde{\mathbf{\Phi}}^{II}_{ijmn}$, $\tilde{\mathbf{\Phi}}^{RI}_{ijmn}$ (defined by (19), (22) and (25)) and $\tilde{\mathbf{\Delta}}^{RR}_{ijmn}$, $\tilde{\mathbf{\Delta}}^{II}_{ijmn}$ (defined by (20) and (23)), respectively, as determined by the polynomial expansion of $E\{\hat{\epsilon}^2\}$ for a particular TED.

Unlike the S-curve for ϕ-QOSTBC, the estimation variance is dependent on the rotation angle ϕ. This is, however, only the case for $\tilde{\mathbf{\Phi}}^{RR}_{ijmn}$, $\tilde{\mathbf{\Phi}}^{II}_{ijmn}$, $\tilde{\mathbf{\Phi}}^{RI}_{ijmn}$ of $\mathbf{\Sigma}_{\tilde{\mathbf{\Phi}}}$ where $i=j$ *and* where i refers to the data symbol from a rotated constellation.

Finally, using (16) and (17), we define the TED SNR as

$$SNR_{TED} = \frac{E^2\{\hat{\epsilon}\}}{\sigma^2_{\hat{\epsilon}}}. \tag{27}$$

C. TED Example

As an example, consider the $N_t = 4$ QOSTBC code $\mathbf{X}_{(q4)}$, which is defined by (2) [1]. The TEM function for $\mathbf{X}_{(q4)}$ can be obtained [6], [10] from the average of the simple combining rule

$$\hat{\epsilon}_{(\text{q4})} = \Re(a_0\zeta_1 - a_1\zeta_0) = a_0^R\zeta_1^R - a_0^I\zeta_1^I - a_1^R\zeta_0^R + a_1^I\zeta_0^I. \tag{28}$$

[1]More examples of TED expressions can be found in [10, Chapter 6].

The TED in (28) corresponds to $\mathcal{S}$ in (8) with $\beta_k = 0\forall k$, $\alpha_1 = -\alpha_2 = 1$, $n_{\alpha,1} = m_{\alpha,2} = 0$, $m_{\alpha,1} = n_{\alpha,2} = 1$.

Substituting the values of $\mathcal{S}$ into (12) and carrying out the matrix multiplications will result in $\mathbf{\Gamma}$ in the form of

$$\mathbf{\Gamma}_{(\text{q4})} = 2\begin{bmatrix} g^\epsilon_{-1}-g^\epsilon_1 & 0 & 0 & -2g^\epsilon_{-2} \\ 0 & g^\epsilon_{-1}-g^\epsilon_1 & 2g^\epsilon_{-2} & 0 \\ 0 & -2g^\epsilon_2 & g^\epsilon_{-1}-g^\epsilon_1 & 0 \\ 2g^\epsilon_2 & 0 & 0 & g^\epsilon_{-1}-g^\epsilon_1 \end{bmatrix}. \tag{29}$$

Examining $\mathbf{\Gamma}_{(\text{q4})}$ in (29), we note that the matrix does not fully satisfy the antisymmetry condition, and hence the resulting TED will be quasi-robust, with the S-curve given by

$$E\{\hat{\epsilon}_{(\text{q4})}\} = 2\rho_2(g^\epsilon_{-1}-g^\epsilon_1) + E_{\mathbf{H}}\{\delta_{\hat{\epsilon}_{(\text{q4})}}\},$$

and a TEM bias of

$$\delta_{\hat{\epsilon}_{(\text{q4})}} = \|\mathbf{H}\|^{-2}\,2\rho_2\sum_{j=1}^{N_r}\big[2\,(g^\epsilon_{-2}-g^\epsilon_2)\Re(h^*_{2j}h_{3j}+h^*_{1j}h_{4j})\big].$$

We now examine the TEM estimation variance. In order to solve for $E^{\mathbf{H}}\{\hat{\epsilon}^2\}$ using (26), we first obtain the components of $\mathbf{\Sigma}_{\tilde{\mathbf{\Phi}}}$ and $\mathbf{\Sigma}_{\tilde{\mathbf{\Delta}}}$ by computing $\hat{\epsilon}^2$ from (28). Squaring (28) will lead to $\mathbf{\Sigma}_{\tilde{\mathbf{\Phi}}}$ in the form of

$$\begin{aligned}\mathbf{\Sigma}_{\tilde{\mathbf{\Phi}}} =& \tilde{\mathbf{\Phi}}^{RR}_{1100}+\tilde{\mathbf{\Phi}}^{RR}_{0011}-2\tilde{\mathbf{\Phi}}^{RR}_{1010}+\tilde{\mathbf{\Phi}}^{II}_{1100}+\tilde{\mathbf{\Phi}}^{II}_{0011} \\ &-2\tilde{\mathbf{\Phi}}^{II}_{1010}-2\tilde{\mathbf{\Phi}}^{RI}_{1100}-2\tilde{\mathbf{\Phi}}^{RI}_{0011}+2\tilde{\mathbf{\Phi}}^{RI}_{1001}+2\tilde{\mathbf{\Phi}}^{RI}_{0110},\end{aligned}$$

where $\tilde{\mathbf{\Phi}}^{RR}_{ijmn}$, $\tilde{\mathbf{\Phi}}^{II}_{ijmn}$ and $\tilde{\mathbf{\Phi}}^{RI}_{ijmn}$ are defined by (19), (22) and (25), respectively. Similarly, the quantity $\mathbf{\Sigma}_{\tilde{\mathbf{\Delta}}}$ for $\mathbf{X}_{(q4)}$ is given by

$$\mathbf{\Sigma}_{\tilde{\mathbf{\Delta}}} = \tilde{\mathbf{\Delta}}^{RR}_{1100}+\tilde{\mathbf{\Delta}}^{RR}_{0011}+\tilde{\mathbf{\Delta}}^{II}_{1100}+\tilde{\mathbf{\Delta}}^{II}_{0011},$$

with $\tilde{\mathbf{\Delta}}^{RR}_{ijmn}$ and $\tilde{\mathbf{\Delta}}^{II}_{ijmn}$ defined by (20) and (23), respectively. We note that since only indices of data drawn from the non-rotated constellation are present, the variance for $\mathbf{X}_{(q4)}$ will be independent of ϕ.

D. Properties of Examples of TEDs

Figures 2 and 3 show the S-curve and TED SNR for $\hat{\epsilon}_{(\text{q4})}$, respectively. The expectation over $\mathbf{H}$ of the TED bias and error variance was computed by simulation by averaging over 10^4

channel instances. In addition, we verify the theoretical curves via simulation, where the data was sampled at a fixed offset with the timing loop disabled. The S-curve and error variance were obtained by averaging $\hat{\epsilon}$ and $(\epsilon - \hat{\epsilon})^2$, respectively, over all code blocks transmitted. Finally, the effect of data decision errors was evaluated by replacing the data symbols in (28) by their corresponding data decisions for SNR $\bar{E}_s/N_0 = 10$ dB and 20 dB, where $\bar{E}_s$ and N_0 denote the average symbol energy, and the noise power spectral density, respectively.

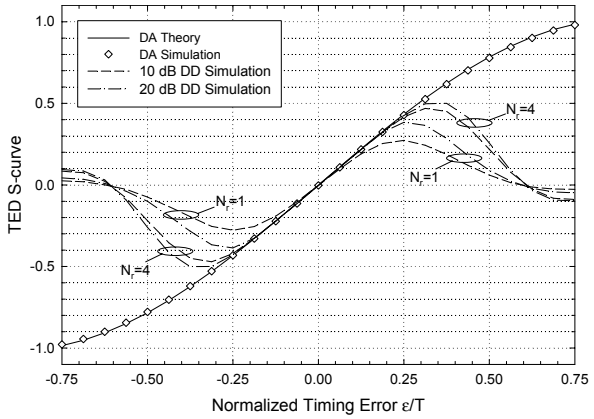

Fig. 2. TED S-curve.

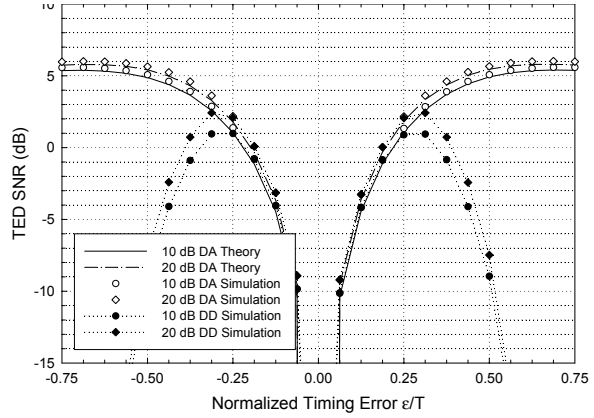

Fig. 3. TED SNR.

We note that in the case of a data-aided TED, the simulated results follow the theoretical expressions very closely. Examining the decision-directed S-curve, we note that incorrect data decisions reduce the linear estimation region to approximately $|\epsilon|/T \approx 0.20$ for SNR of 20 dB, with the range extended to $|\epsilon|/T \approx 0.30$ with increased diversity order. While the linear estimation range in Figure 2 is sufficient for timing loop operation, it is approximately 20% smaller than that for OSTBC TEDs [10]. This can be attributed to the use of approximate decision variables in (5) in timing estimation.

Finally, we should note that the property evaluated in Figure 3 is the output SNR of the TED, which constitutes the *input* SNR of the timing loop. Since the timing loop performs an averaging operation by virtue of the loop filter and the threshold device, the TED SNR will be significantly increased by virtue of the integration process.

IV. System Simulations

We present simulation results evaluating the performance of receiver employing the TED $\hat{\epsilon}_{(q4)}$ in its timing loop [2]. We consider frequency-flat Rayleigh fading with a normalized Doppler frequency of $f_D T = 0.01$. It is assumed that the receiver has performed coarse timing acquisition, which would typically be done via a training sequence. The timing drift was simulated by perturbing the sampling phase τ_l, where the interval between timing slips, measured in symbol intervals and denoted by N_τ, was modeled by a Gaussian random variable, with a mean of $\bar{N}_\tau$ and a variance $\sigma^2_{N_\tau} = 0.1\bar{N}_\tau$. The drift direction was random and equiprobable, and the step size fixed to $T/16$. The mean normalized timing error bandwidth is given by

$$\bar{B}_\tau T = \frac{T/16}{\bar{N}_\tau T} = \frac{1}{16\bar{N}_\tau}.$$

Timing estimation was done using the TED given by (28). Since the focus of the investigation is the tracking performance of the detector, the timing estimation was done without the data knowledge at the receiver. Hence the data symbols a_m in (28) were replaced by their estimates $\hat{a}_m$. The timing error estimate for code block l, that is $\hat{\epsilon}_l$, was passed through a first-order, IIR, timing loop filter with the output of

$$\hat{\epsilon}'_l = \alpha\hat{\epsilon}'_{l-1} + (1-\alpha)\hat{\epsilon}_l,$$

where the loop constant $\alpha = 0.9$. When $\hat{\epsilon}'_l$ exceeded a threshold value $\epsilon_{th} = 0.25$, the timing correction $\hat{\tau}_l$ was adjusted by a fraction of the symbol interval $T/8$, according to the polarity of the error estimate.

In addition to the receiver with perfect channel knowledge, we evaluate the effects of channel estimation errors for a pilot symbol assisted modulation (PSAM) receiver, as described in [1]. The data was divided into frames consisting of known orthogonal pilot blocks, followed by 4 OSTBC data code blocks. The received sequence was decimated to recover the pilot symbols, which were used to obtain the channel estimates for the pilot slots. These were subsequently interpolated to obtain channel fading values for the data portion of each frame. In the results presented here, Wiener interpolation filter with 9 interpolants was used.

In Figure 4 we present SER performance for timing drift bandwidth $\bar{B}_\tau T = 10^{-4}$ [3]. Results for channel state information at the receiver (CSIR) and PSAM receivers are presented, in addition to reference curves for perfect channel and timing estimation, and perfect timing with PSAM channel estimation.

The results demonstrate that the CSIR receiver, which was assumed in the TED design process, is able to track the timing

[2]For detailed description of the simulation setup as well as additional results, the reader is referred to [6] [10, Chapter 5].

[3]Current state of the art temperature compensated crystal oscillators (TCXOs) have a frequency stability of well under 10 ppm, corresponding to $\bar{B}_\tau T < 10^{-5}$ [11]. SER results for varying values of $\bar{B}_\tau T$ can be found in [10, Chapter 6].

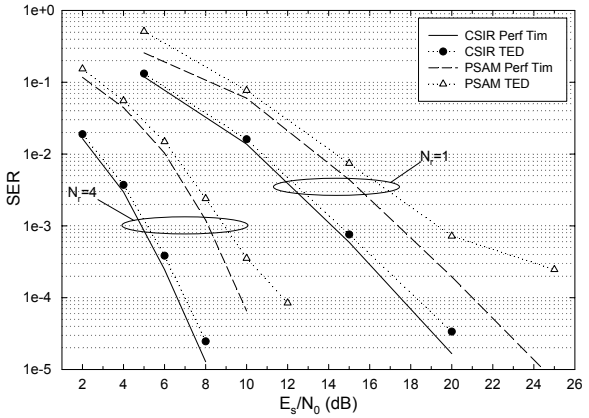

Fig. 4. QPSK SER Performance.

variation with a performance drop of only 0.5 dB. In the case of PSAM receiver, the SER performance exhibits degradation in the high SER region. By observing the reference curves for perfect timing with PSAM channel estimation, we note that the TED performance is sensitive to the channel estimation errors. Since the performance for the CSIR receiver is very good, we conclude that improved channel estimation technique should be considered.

V. Conclusion

We have presented the design and analysis of QOSTBC TEDs, showing that a low complexity timing measurement can be obtained by operating on data symbols and approximate decision variables. The S-curve, estimation variance and TED SNR were solved for under ideal conditions. Simulation results were used to analyze the above properties with decision errors, and to evaluate the system performance including the effects of channel estimation. SER results showed a timing synchronization loss for CSIR of under 0.5 dB.

Appendix I

We evaluate the expectation of the general form of TED given in (7) by considering $E^{\mathbf{H}}\{\tilde{a}_n\tilde{\zeta}_m\}$ and $E^{\mathbf{H}}\{\tilde{a}_n\tilde{\zeta}_m^*\}$ [4]. Using (5) and (3), we can write

$$E^{\mathbf{H}}\{\tilde{a}_n\tilde{\zeta}_m\} = \|\mathbf{H}\|^{-2}\,\mathrm{tr}\Big\{\mathbf{A}_m\mathbf{G}_\epsilon^H E^{\mathbf{H}}\left\{\tilde{a}_n\Re(\tilde{\mathbf{X}}^H\mathbf{H}^H\mathbf{H})\right\} -j\mathbf{B}_m\mathbf{G}_\epsilon^H E^{\mathbf{H}}\left\{\tilde{a}_n\Im(\tilde{\mathbf{X}}^H\mathbf{H}^H\mathbf{H})\right\}\Big\},$$

which can be expanded to [10, Chapter 6]

$$\begin{aligned}E^{\mathbf{H}}\{\tilde{a}_n\tilde{\zeta}_m\} =&\|\mathbf{H}\|^{-2}\times\\ &\mathrm{tr}\Big\{\mathbf{A}_m\mathbf{G}_\epsilon^H\Big[E\big\{\Re(\tilde{a}_n^R\tilde{\mathbf{X}}^H)+j\Re(\tilde{a}_n^I\tilde{\mathbf{X}}^H)\big\}\Re(\mathbf{H}^H\mathbf{H})\\ &\quad -E\big\{\Im(\tilde{a}_n^R\tilde{\mathbf{X}}^H)+j\Im(\tilde{a}_n^I\tilde{\mathbf{X}}^H)\big\}\Im(\mathbf{H}^H\mathbf{H})\Big]\\ &-j\mathbf{B}_m\mathbf{G}_\epsilon^H\Big[E\big\{\Im(\tilde{a}_n^R\tilde{\mathbf{X}}^H)+j\Im(\tilde{a}_n^I\tilde{\mathbf{X}}^H)\big\}\Re(\mathbf{H}^H\mathbf{H})\\ &\quad +E\big\{\Re(\tilde{a}_n^R\tilde{\mathbf{X}}^H)+j\Re(\tilde{a}_n^I\tilde{\mathbf{X}}^H)\big\}\Im(\mathbf{H}^H\mathbf{H})\Big]\Big\}.\end{aligned} \tag{30}$$

[4] A more detailed derivation is presented in [10, Chapter 6].

Reversing the order of $\Re\{\cdot\}$ and $\Im\{\cdot\}$ with the expectation operator $E\{\cdot\}$, we now solve for $\Re\{E(\tilde{a}_n^R\tilde{\mathbf{X}}^H)\}$, $\Re\{E(\tilde{a}_n^I\tilde{\mathbf{X}}^H)\}$, $\Im\{E(\tilde{a}_n^R\tilde{\mathbf{X}}^H)\}$ and $\Im\{E(\tilde{a}_n^I\tilde{\mathbf{X}}^H)\}$. While one must distinguish between the cases for non-rotated constellations ($n = 1, 2$) and rotated ones ($n = 3, 4$), it can be shown that the expectations in (30) are independent of the rotation angle ϕ [10, Chapter 6]. Using (1), one can show that

$$\begin{aligned}\Re\big\{E\{\tilde{a}_n^R\tilde{\mathbf{X}}^H\}\big\} &= \Re\Big\{E\Big\{\tilde{a}_n^R\sum_{m=0}^{N_s-1}\tilde{a}_m^R\mathbf{A}_m^H - j\tilde{a}_m^I\mathbf{B}_m^H\Big\}\Big\}\\ &= E\{(a_n^R\cos(\phi)-a_n^I\sin(\phi))^2\}\mathbf{A}_n^H\\ &= \rho_2\mathbf{A}_n^H,\end{aligned} \tag{31}$$

where we used the fact that $E\{a_n^Ra_m^R\} = 0$ for $m \neq n$. The last equality, which assumes $E\{(a_n^R)^2\} = E\{(a_n^I)^2\} = \rho_2$, holds true since since $E\{a_n^Ra_n^I\} = 0$. Using the same approach, we have

$$\Im\big\{E\{\tilde{a}_n^I\tilde{\mathbf{X}}^H\}\big\} = -\rho_2\mathbf{B}_n^H, \tag{32}$$

and, finally, $\Re\big\{E\{\tilde{a}_n^I\tilde{\mathbf{X}}^H\}\big\} = 0$, $\Im\big\{E\{\tilde{a}_n^R\tilde{\mathbf{X}}^H\}\big\} = 0$

Substituting (31) and (32) into (30), after some algebraic manipulation, taking the real part of (30) results in (9). The solution to $E^{\mathbf{H}}\{\tilde{a}_n\tilde{\zeta}_m^*\}$ can be obtained using the same approach as for $E^{\mathbf{H}}\{\tilde{a}_n\zeta_m\}$.

References

[1] A.F.Naguib, V.Tarokh, N.Seshadri, and R.Calderbank. A space-time coding modem for high-data-rate wireless communications. *IEEE J. Select. Areas Commun.*, 16(8):1459–1478, October 1998.

[2] Y.-C.Wu, S.C.Chan, and E.Serpedin. Symbol-timing synchronization in space-time coding systems using orthogonal training sequences. In *Proc. IEEE WCNC*, pages 1205–1209, March 2004.

[3] K.Rajawat and A.K.Chaturvedi. A low complexity symbol timing estimator for MIMO systems using two samples per symbol. *IEEE Communications Letters*, 10(7):525–527, July 2006.

[4] P.A.Dmochowski and P.J.McLane. Robust timing epoch tracking for Alamouti space-time coding in flat Rayleigh fading MIMO channels. In *Proc. IEEE International Conference on Communications (ICC)*, pages 2397–2401, May 2005.

[5] P.A.Dmochowski and P.J.McLane. On the properties of robust timing error detector for Alamouti space-time coding in flat Rayleigh fading MIMO channels with randomly distributed timing drift. In *Proc. IEEE Global Telecommunications Conference (GLOBECOM)*, pages 193–198, November-December 2005.

[6] P.A.Dmochowski and P.J.McLane. Timing error detector design for orthogonal space-time block coded receivers. In *Proc. 16th IEEE International Symposium on Personal, Indoor and Mobile Radio Communications (PIMRC)*, September 2006.

[7] V.Tarokh, H.Jafarkhani, and A.R.Calderbank. Space-time block codes from orthogonal designs. *IEEE Trans. Inf. Theory*, 45:1456–1467, July 1999.

[8] H.Jafarkhani. *Space-Time Coding - Theory and Practice*. Cambridge University Press, New York, 2005.

[9] G.Ganesan and P.Stoica. Space-time block codes: A maximum SNR approach. *IEEE Trans Inf. Theory*, 47(4):1650–1656, May 2001.

[10] P.A.Dmochowski. *Design and Analysis of Pulse-Shaped Space-Time Block Coding Based Symbol Timing Recovery Algorithms*. PhD thesis, Queen's University, Kingston, Canada, September 2006. Available at www.ece.queensu.ca/directory/laboratories/qwcl/thesis.html or www.paweldmochowski.com.

[11] W.Zhou, H.Zhou, Z.Xuan, and W.Zhang. Comparison among precision temperature compensated crystal oscillators. In *Proc. IEEE International Frequency Control Symposium and Exposition*, pages 575–579, August 2005.